Improving AUV Thruster Performance: Optimizing Hydrodynamic Nose-Cone Section with Automated Genetic Algorithm and Computational Fluid Dynamics Integration

Manuel Chad G. Agurob[1]* and Sherwin A. Guirnaldo[2]
[1]Electronics Technology Department
Bukidnon State University
Malaybalay City, Bukidnon 8700 Philippines
**manuel_chad@buksu.edu.ph*

[2]Mechanical Engineering Department
Mindanao State University – Iligan Institute of Technology
Iligan City, Lanao del Norte 9200 Philippines

Date received: December 31, 2023
Revision accepted: June 10, 2026

Abstract

To maximize the speed of Autonomous Underwater Vehicles (AUVs), it is crucial to carefully consider the design of the conical nose, situated at the forefront of the underwater thruster. The study introduces a method that significantly increases the thruster-generated output velocity by optimizing the curvature of the cone's spline and the length of the conical nose geometry using a Genetic Algorithm (GA). This optimization process facilitates real-time interactions between the GA and Computational Fluid Dynamics (CFD)-based simulations, permitting dynamic adjustments to the design parameters. The GA utilizes velocity metrics derived from fluid flow analysis in CFD simulations as a criterion for fitness. Informed by this criterion, the GA generates new design iterations, which undergo further CFD simulations for continued evaluation and refinement. This iterative process identifies promising combinations of conical nose shape and length for improving thruster output velocity. Through this analysis two intermediate nose cone prototypes were generated. The study found that modifications to the nose cone geometry increased the thruster output velocity from a baseline of approximately 5.05 m/s to a maximum value of 5.41 m/s among the evaluated configurations, representing a 7.13% improvement. This configuration was identified as the best-performing nose cone geometry in terms of output velocity within the investigated design space.

***Keywords**:* autonomous underwater vehicle (AUV), computational fluid dynamics (CFD), conical nose design, design optimization, genetic algorithm (GA)

---

1. Introduction

The design and evolution of the nose cone of an Autonomous Underwater Vehicle (AUV) have been critical in reducing hydrodynamic drag and facilitating smooth flow over the vehicle's body. It is the primary interface between the vehicle and its aquatic environment. It is the leading point of contact with water where the hydrodynamic design of underwater gliders emphasizes the importance of nose cone design in reducing drag and facilitating natural laminar flow without compromising practical aspects like payload capacity (Lidtke *et al*., 2018). A bullet nose and sharp tail improve the hydrodynamic performance of an AUV, showcasing the impact of nose cone design on overall vehicle efficiency (Divsalar, 2020) and the importance of AUV nose cones for hydrodynamic drag reduction in efficiently designing hull shapes with minimum drag (Liu *et al*., 2017). Traditional nose cone design typically relies on empirical knowledge and basic flow models. However, using advanced computational tools makes refining these designs possible for optimal performance. Such computational techniques apply genetic algorithms (GA) in conjunction with computational fluid dynamics (CFD) to optimize the nose cone shape, specifically in its integration with the AUV's thruster section. Inspired by natural selection and genetics principles, genetic algorithms provide a robust framework for handling complex optimization problems with multiple objectives and many design variables (Maruyama *et al*., 2018). When paired with CFD-based flow simulations, which offer detailed insights into the fluid dynamics around the vehicle, a powerful toolset emerges for the design optimization process (Vasudev *et al*., 2018). The thruster section's performance heavily depends on the quality of flow it receives, which in turn is influenced by the shape of the nose cone. An optimized nose cone shape can ensure that the flow to the thruster is uniform and free of disturbances, which can significantly improve the efficiency and lifespan of the propulsion system. Recent research has shown a growing interest in optimizing the nose cone shape of Autonomous Underwater Vehicles (AUVs) using a genetic algorithm and CFD-based flow simulation. The aim is to enhance the AUVs' hydrodynamic performance and reduce drag force. This line of analysis focuses on exploring the design of elliptical cone shapes for the nose and tail of AUV hulls to achieve improved hydrodynamic performance (Saghafi *et al*., 2020).

On the water's surface, unmanned surface vehicles (USVs), also known as autonomous surface vehicles (ASVs), operate without a crew. These are significantly less expensive than comparable weather and research vehicles.

USV primarily conducts exploration missions in an underwater environment where surveillance, data collection, maintenance, and repair of underwater structures are completed. On the surface of the water, USVs distinguish themselves from other unmanned aquatic platforms for data collection due to their access to the Global Positioning System (GPS) and different localization strategies (Matias *et al*., 2015; Han *et al*., 2016), superior communication capabilities compared to other marine vehicles (Kartha *et al*., 2015; Luo *et al*., 2017). An unmanned surface vehicle is segmented based on its application, size, hull type, propulsion system, modes of operation, endurance, payload, and geography during its design. The propulsion systems of amphibious robots are crucial to achieving these diverse applications in a complicated environment (Masmitja *et al*., 2018). According to (Chung *et al*., 2013), modeling the thruster is required for efficient system control of an underwater water vehicle. Simulating the thruster's thrust force for a specific design and application is essential. The thrust force is the most influential factor in the system.

Moreover, the application of Genetic Algorithms and CFD for flow control optimization has been a key area of development, with studies such as Kotragouda (2007) demonstrating the integration of these tools to guide the movement of jets along the airfoil's upper surface and determine near-optimal control values within a specified range. Furthermore, the suitability of using CFD tools, such as ANSYS-CFX, as an initial analysis tool for predicting the drag and thrust power of underwater disk robots has been examined in the study by Joung *et al*. (2014).

Previous studies on hydrodynamic improvement of AUVs have predominantly addressed full-hull shape refinement (Divsalar, 2020; Saghafi & Lavimi, 2020) or propeller-level performance and thrust prediction (Joung *et al*., 2014), with comparatively little emphasis on the integration zone between the nose cone and the thruster section. Existing GA-based optimization studies in related domains (Kotragouda, 2007; Vasudev *et al*., 2018) generally rely on manual or semi-automated loops, in which geometry updates and CFD evaluations are only partially scripted. Gradient-free optimization methods, particularly GA–CFD frameworks, nonetheless remain widely adopted because they can accommodate highly nonlinear design spaces, mixed design variables, and multiple objectives without requiring derivative information from the flow solver (Maruyama *et al*., 2018).

In parallel, gradient-based approaches have gained increasing prominence in underwater vehicle design. Saghafi & Lavimi, (2020) employed a continuous adjoint solver within a gradient-based framework to optimize an AUV hull, while Bhuiyan *et al*. (2025) combined an adjoint method with Proper Orthogonal Decomposition (POD) to enhance AUV hydrodynamic efficiency using Reynolds-averaged Navier–Stokes (RANS)-based CFD. Multi-surrogate and gradient-based strategies have also been proposed for hydrodynamic shape optimization of autonomous and remotely operated vehicles, further demonstrating the potential of systematic shape refinement in underwater applications (Liu *et al*., 2017). Collectively, these adjoint and gradient-based formulations offer efficient sensitivity information and are particularly attractive for high-dimensional hull optimization but typically require direct access to solver internals. By contrast, the GA employed in the present study is a fully gradient-free optimizer that does not rely on adjoint or Jacobian information, which makes it directly compatible with commercial CFD packages such as SOLIDWORKS Flow Simulation that do not natively expose adjoint capabilities.

Integrating the nose cone with the thruster section is a distinct task that requires careful consideration. The thruster section's performance heavily depends on the quality of flow it receives, which in turn is influenced by the shape of the nose cone. An optimized nose cone shape can ensure that the flow to the thruster is uniform and free of disturbances, which can significantly improve the efficiency and lifespan of the propulsion system. This study explores the interacting application of genetic algorithms and CFD-based flow simulations to pursue an optimal nose cone design to increase the output velocity of the thruster. The key contributions and novelty of this study are as follows: fully automated real-time GA-CFD coupling through MATLAB-SOLIDWORKS integration, eliminating manual iteration and operator bias in the optimization loop (1); simultaneous optimization of two geometric parameters — spline curvature (c) and nose cone length (l) — enabling a broader design space exploration than single-variable approaches (2); application of optimization to the thruster-integrated nose cone section, addressing a gap in the literature where prior work has focused on standalone hull or nose shapes rather than the nose-cone-to-thruster transition zone (3).

2. Methodology

2.1 Simple Momentum Theory

Figure 1 presents a simplified depiction of a propeller's operational dynamics, grounded in momentum theory. This theory elucidates the transformation of the propeller's momentum and kinetic energy. According to this framework, the optimal propeller speed and its most efficient utilization are identified as follows: a nose cone is strategically positioned at the forefront of the propeller, designed to maximize the acceleration of flow that the propeller can generate. This arrangement significantly mitigates the turbulent flow typically observed within the thruster.

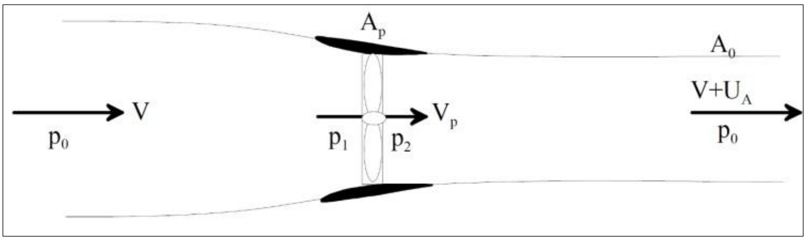

Figure 1. A simple momentum theory showing velocity changes applied in a propeller

Consequently, this leads to a decrease in the thruster's drag force, thereby enhancing the efficiency of the outflow speed. Equation 1 articulates the variation in momentum, providing a mathematical expression for the thrust generated.

$$T = \rho \cdot Q \cdot UA \quad (1)$$

Where *T* is the change in Momentum; *Q* = APVP =Volume flow through the propeller; *VP* is the velocity through the propeller disk; AP = area of the propeller disk; *UA* = Added velocity in the flow behind the propeller

Through Bernoulli's Equation, expressions for pressure in front of and behind the propeller are obtained:

$$\Delta p_1 = \frac{1}{2}\rho\left[V_p^2 - V^2\right] \quad (2)$$

$$\Delta p_2 = \frac{1}{2}\rho\left[(V - U_A)^2 - {V_p}^2\right] \quad (3)$$

Combining Equations 2 and 3 the propeller thrust can be expressed as:

$$T_p = A_p(\Delta p_1 + \Delta p_2) = \rho A_p \left(V + \frac{1}{2}U_A\right) \cdot U_A \tag{4}$$

where T_p is the propeller thrust, A_p is the propeller disk area, Δp_1 and Δp_2 are the pressure differences across the propeller, ρ is the fluid density, V is the inflow velocity, and U_A is the added velocity generated by the propeller. Equation 4 shows that the thrust depends on the propeller disk area, fluid density, inflow velocity, and the added velocity imparted to the fluid. Therefore, improving the flow through the nose cone can increase the added velocity and enhance the resulting propeller thrust

Equation 5 expresses the volumetric flow rate through the propeller disk:

$$Q = A_p \left(V + \frac{1}{2}U_A\right) \tag{5}$$

where Q is the volumetric flow rate, A_p is the propeller disk area, V is the inlet flow velocity, and U_A is the velocity added by the propeller

Dividing Equation 5 by the propeller disk area gives the average flow velocity through the propeller disk:

$$V_p = \frac{Q}{A_p} = \left(V + \frac{1}{2}U_A\right) \tag{6}$$

where V_p is the average velocity through the propeller disk

The hydrodynamic shape of the nose cone influences the flow entering the propeller and, consequently, the thruster output velocity. A flat front cap may cause additional drag and flow disturbances as the thruster moves through water. Installing a properly shaped nose cone ahead of the propeller can guide the incoming flow more smoothly, reduce flow separation, and improve the velocity through the propeller disk. In this study, the added velocity, U_A, is therefore used as a performance parameter for evaluating the effects of nose cone geometry. Rearranging Equation 6 gives Equation 7:

$$U_A = 2\left(V_p - V\right) = 2\left(\frac{Q}{A_p} - V\right) \tag{7}$$

2.2 The 3D Geometric Model

This study identifies the best-performing nose cone geometry in terms of average output velocity within the investigated design space. It uses a Genetic Algorithm (GA) and CFD simulation to optimize the nose-cone shape, expecting increased output velocity through the propeller disk.

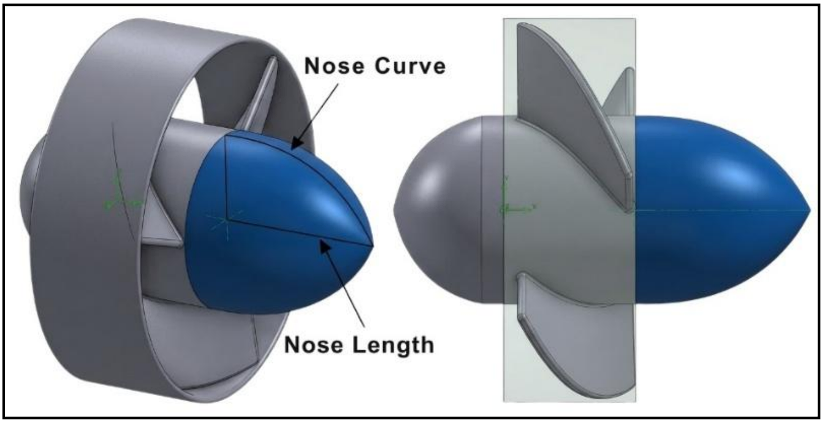

Figure 2. Nose cone section in a thruster

This work adapts the geometry of a commercially available thruster (Huynh, 2016) to propel robotic unmanned surface vehicles (USVs). These USVs can easily maneuver around anything that floats due to the flexibility of the thruster's design. Since the nose drag does not affect the tail drag, it is permissible to use any nose on a body with various tails (Saghafi & Lavimi, 2020). Therefore, this work will focus on the immediate effect of the nose cone on the optimization of output flow speed, as revealed in Figure 3. Accuracy of the results is obtained from the numerical solutions generated by SOLIDWORKS and MATLAB. This software actively modifies the geometry of the nose cone by automatically interacting with and instantly evaluating each shape candidate. Its seamless interaction helps to identify the optimized nose cone shape for the thruster. MATLAB's genetic algorithm processes the velocity using the fitness rating SOLIDWORKS Flow Simulation generates for the thruster.

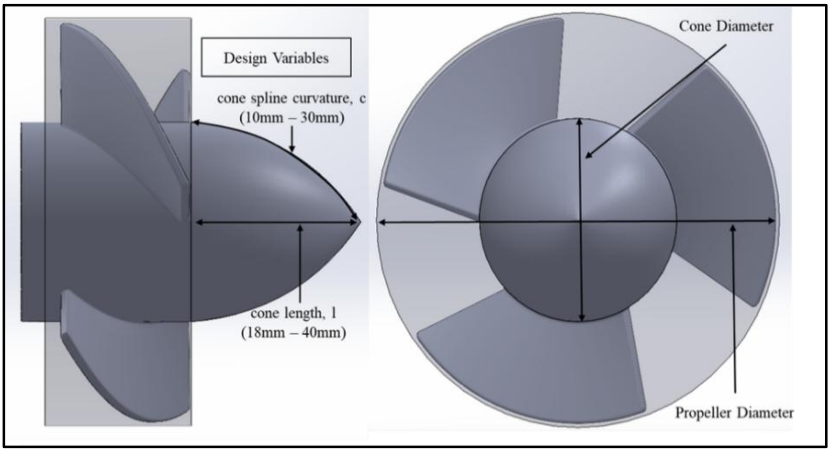

Figure 3. The proposed thruster geometry shows its nose cone section and its sizes

The creation of the CAD geometric model took place in SOLIDWORKS. A spline sketch forms a shape by continuously altering its curvature, creating a design not achievable with straight lines and circles. The method interpolates two points to create a smooth and flowing sketch of the nose cone's curve, representing it numerically. This method endows the body with flexibility. Thus, the spline sketch facilitates exploring various shape variations during the Genetic Algorithm (GA) search for optimizing the cone's curved shape and length. Consequently, the design variables are the nose cone length (l) and curvature (c).

The design parameters spline curve, c, and nose cone length, l, determine the velocity as a fitness rating. In SOLIDWORKS, the spline curve adjusts the nose cone's geometric curve from 10 mm to 30 mm, and the nose cone length extends from 18 mm to 40 mm. Adjusting these design variables necessitates a search for the optimal propeller output velocity rating. In response, MATLAB's genetic algorithm provides SOLIDWORKS with parameter candidates and performs a Computational Fluid Dynamic (CFD) analysis. This software solves for the surface goal average velocity or the thruster's output flow speed. The CFD analysis assesses how the nose cone shape affects the ambient static fluid relative to the thruster's rotating frame or propeller. The solver employs the Favre-averaged Navier-Stokes equations, which are formulations of mass, momentum, and energy conservation laws for fluid flows (Dassault Systèmes, 2021). For turbulent flow prediction, these equations are supplemented by a modified k-ε turbulence model with damping functions, enabling automatic resolution of both laminar and turbulent flow regimes without requiring manual specification of the transition point. Moreover, the boundary conditions for rotational velocity (rotating region), wall, and pressure follow the geometric parameters in Table 1. Finally, the study identifies the configuration with the highest output velocity among the evaluated nose cone geometries.

Table 1. Thruster geometric parameters

Parameter	Value
Propeller diameter	80mm
Number of blades	Z=3
Thruster Length	75mm
Rotational Speed	323 rad/s (3084 rpm)

CFD is commonly employed to simulate and analyze the hydrodynamic performance and dynamic behavior of thrusters. This simulation accurately shows the impact of changes in the nose cone's shape on the output velocity flow. The process employs a MATLAB function named GA and utilizes SOLIDWORKS to calculate the thruster's output velocity to identify the configuration with the highest output velocity among the evaluated candidates. The SOLIDWORKS Simulation Flow feature is crucial in generating the thruster's speed. When applying the GA, the analysis should suggest a geometry that closely resembles the desired shape of the thruster's nose cone.

2.3 Establishment of Domain Computation

The SOLIDWORKS computational domain specifies the geometric details and boundary conditions. This domain calculates the propeller's output speed, which varies based on the nose cone's shape and the fluid flow direction into the thruster during constant propeller rotation. Figure 4 shows the dynamic fluid domain zone that simulates the propeller's counterclockwise (CCW) rotation.

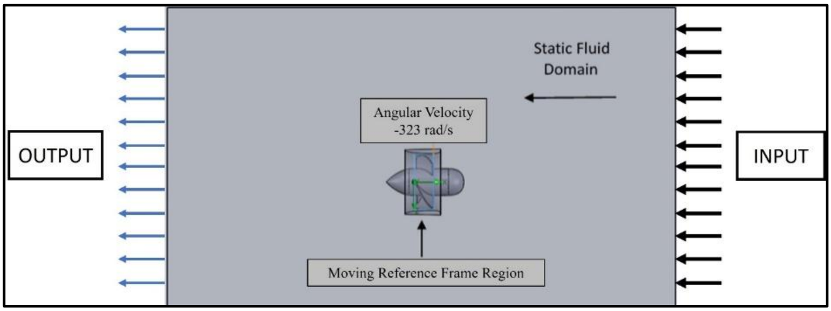

Figure 4. Simplified 3D thruster model inside the computational domain

The remainder of the computational domain is a static fluid region simulating open-water conditions. The boundaries include a surrounding pressure boundary and a constant inlet velocity of 0.02 m/s. In the virtual environment, the walls and the nozzle's outflow have no specified direction. The hydrodynamic domain does not include gravity or buoyancy. The constant inlet velocity of 0.02 m/s represents near-quiescent conditions consistent with bollard-pull testing, a standard approach for evaluating thruster performance in isolation (Chung *et al*., 2013). Gravity and buoyancy are excluded because this study focuses on the hydrodynamic effect of nose-cone geometry on output velocity, not on vehicle-level trajectory or depth-dependent behavior. These simplifications are consistent with established thruster characterization methodology (Joung *et al*., 2014). Based on the propeller diameter (D = 80 mm) and the inlet velocity (V = 0.02 m/s), the Reynolds number at the inlet is $Re = \rho VD/\mu \approx 1{,}594$, indicating laminar inflow conditions. At the propeller disk, where the output velocity reaches 5.41 m/s, the Reynolds number increases to approximately 430,778, confirming a fully turbulent regime in the wake region. This transition from laminar inflow to turbulent outflow is consistent with the solver's automatic laminar-turbulent handling via the modified k-ε model.

The simulation employs a steady-state formulation with a Moving Reference Frame (MRF) to model the propeller's rotation at a constant angular velocity of 323 rad/s. The MRF approach is appropriate for evaluating time-averaged thruster performance at a fixed rotational speed and is computationally efficient compared to transient sliding-mesh methods, which would be required for time-resolved analysis of blade-passing effects. By conducting a CFD analysis, the output velocity can be examined without the need for complex experimental setups. This analysis focuses on studying how different nose cone shapes impact the thruster. The CFD simulation conditions are set in the fluid computational domain to analyze the external velocity relative to the model's rotating frame and CFD boundary conditions are shown in Table 2. The adiabatic wall pressure and temperature are established at 101325 Pa and 293.2 K, respectively.

Table 2. Summary of CFD boundary conditions

Boundary	Type	Value
Inlet	Velocity inlet	0.02 m/s
Surrounding pressure	Pressure boundary	101,325 Pa
Walls	Adiabatic no-slip	Real wall condition
Rotating region	Moving Reference Frame	323 rad/s (CCW)
Fluid medium	Water at 20 °C	ρ = 998.2 kg/m^3, μ = 1.002 × 10^{-3} Pa·s
Initial temperature	Isothermal	293.2 K

The CFD input includes the rotating region, a velocity surface goal, and a real wall condition behind the propeller. A moving reference region is configured for the domain's inner area, with the propeller's rotational velocity set at a fixed value of 323 rad/s. The CFD solver parameter stopping conditions are set to 120 iterations at automatic iteration per travel or when all set goals converge. With global mesh settings on automatic, the total cells in contact with the solids are 3,478 at the optimized shape, and the total fluid meshed cell count is 51,760. The solver's iterative convergence criterion was satisfied, with the surface velocity goal converging to within 0.000916 m/s — a variation of 0.017% relative to the computed output velocity. This convergence behavior, combined with the solver's automatic initial mesh refinement at solid/fluid interfaces and curvature regions (Dassault Systèmes, 2021, p. 98), supports the reliability of the mesh configuration employed. Table 2 summarizes the key boundary conditions applied in the CFD simulation.

2.3.1 Grid-Sensitivity Assessment

A post-optimization grid-sensitivity assessment was conducted using optimal design candidate to evaluate the sensitivity of the predicted average output velocity to grid resolution. The nose cone geometry, computational domain, fluid properties, inlet velocity, propeller rotational speed, turbulence model, boundary conditions, surface-goal measurement plane, and solver-convergence criteria were maintained consistently in all simulations.

Three manually defined global meshes were evaluated using divisions of $24 \times 24 \times 24$, $32 \times 32 \times 32$, and $43 \times 43 \times 43$, representing the coarse, medium, and fine meshes, respectively. For each mesh level, the total number of fluid cells, number of fluid cells contacting the solid surfaces, converged average output velocity, iteration count, and computation time were recorded.

The percentage difference between successive mesh levels was calculated as the absolute difference between the average output velocities of the current and next finer meshes, divided by the velocity obtained using the next finer mesh, and expressed as a percentage.

2.4 Implementation Design

Calculating the output flow speed in meters per second (Angular velocity) involves using SOLIDWORKS Flow Simulation. The first step in integrating SOLIDWORKS with MATLAB consists of writing a script in MATLAB that retrieves the iterated average velocity from the batch file generated by the SW Flow Simulation. The next step is linking MATLAB's Genetic Algorithm (GA) results with SOLIDWORKS. This linkage happens through MATLAB scripting, connecting potential parameters to the SOLIDWORKS equation link text file. Macro recording software plays a crucial role in automating the analysis in the Flow Simulation. This setup allows for the return of input parameters to MATLAB, as demonstrated in Figure 5.

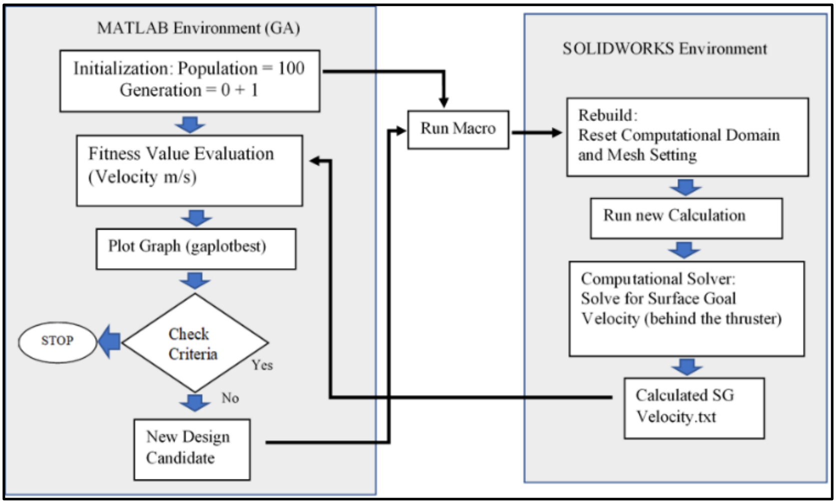

Figure 5. Overview of computational methodology

2.5 Optimization Process

Evaluating individuals within each generation's population is considered a boundary constraint. The design variables have limits set by lower and upper geometrical boundary constraints, as displayed in Figure 3. The velocity-dependent function guides the optimization model toward the length and curvature of the nose cone. The optimization focuses on determining the ideal numerical values for the cone's spline curvature and length. Equation 8 details the objective function, constraints, and design variables regarding maximum output velocity.

$$\begin{aligned} &\max_{c,l} V(c, l) \\ &\text{subject to } 10 \leq c \leq 30 \text{ mm}, \\ &\qquad 18 \leq l \leq 40 \text{ mm}, \end{aligned} \tag{8}$$

where $V(c, l)$ is the thruster output velocity obtained from the CFD simulation, $c$is the nose cone spline curvature, and $l$is the nose cone length. As expressed in Equation 8, the optimization objective is to determine the combination of c and l that produces the maximum output velocity within the prescribed geometric limits. For implementation in the MATLAB Genetic Algorithm, the maximization problem is converted into the equivalent minimization form, $f(c, l) = -V(c, l)$, because the algorithm searches for the minimum fitness value. For each candidate design, MATLAB updates the nose cone geometry, initiates the CFD simulation, and evaluates the resulting output velocity. The iterative process continues until the stopping criterion is satisfied and the best-performing configuration within the prescribed geometric limits is identified.

Average output velocity was selected as the optimization objective because the study specifically investigates the influence of nose cone geometry on flow acceleration through the thruster. With the propeller diameter, rotational speed, fluid properties, computational domain, and boundary conditions held constant, the surface-average velocity measured behind the propeller provides a consistent scalar fitness value for comparing the GA-generated nose cone configurations. This objective is also aligned with the momentum-theory formulation adopted in the study, in which changes in flow velocity represent the additional momentum imparted to the fluid. However, output velocity alone does not provide a complete assessment of overall thruster performance. Other important parameters, including thrust, propulsive efficiency, pressure loss, shaft torque, power consumption, and cavitation susceptibility, were not incorporated into the objective function. Therefore, the selected configuration is interpreted as the best-performing nose cone geometry in terms of output velocity within the investigated design space, rather than as the globally optimal thruster design.

The boundary constraints preserve the nose cone's geometric flexibility while enabling the Genetic Algorithm (GA) to search for the optimal solution within the specified design domain. These constraints also help prevent invalid geometries, such as warping of the nose cone tip when the length exceeds the corresponding spline curvature. The GA searches for the optimal combination of the two design variables—spline curvature and nose cone length—within their prescribed limits. At each iteration, the system verifies the constraints, generates a candidate set of design variables, and updates the nose cone geometry accordingly. SOLIDWORKS Flow Simulation then evaluates the candidate design and computes the corresponding average output velocity. This velocity is returned to the MATLAB GA as the fitness value for generating the next set of design candidates. The iterative process continues until the stopping criterion is satisfied or the predetermined number of generations is reached, as illustrated in Figure 6.

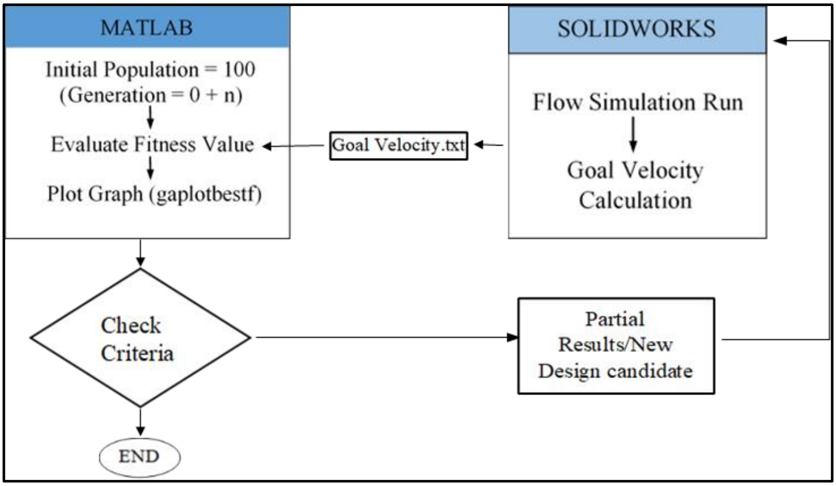

Figure 6. Flow diagram of the optimization process

3. Results and Discussions

To establish confidence in the numerical model, the baseline thruster configuration was compared against published performance data. Blue Robotics (2017) reports a theoretical maximum flow speed of approximately 3.80 m/s at 12V for the T200 thruster at approximately 3,075 RPM. The present simulation, operating at 3,084 RPM with an optimized nose cone, yields an output velocity of 5.41 m/s. The published T200 data provide a contextual performance comparison rather than a direct validation of the simulated output velocity. The higher output velocity is attributable to the flow-directing effect of the nose cone, which accelerates and streamlines the flow through the thruster duct. Independent experimental characterization of the T200 by Lam *et al*. (2023) confirmed that measured bollard thrust agrees within 5% of manufacturer specifications, supporting the reliability of the T200 thruster model upon which this study builds.

Following is a description of the thruster's output velocity based on the optimized nose cone shape. The CFD analyzes the thruster's hydrodynamic properties concerning the newly designed nose cone shape. The CFD solver parameter stops at 120 iterations per automatic travel or when all configured surface velocity goals converge. The analysis reveals the enhanced flow velocity caused by the propeller. This analysis presents the pressure distribution on the blades and the velocity distribution in the thruster to improve understanding of the thruster's characteristics.

The optimization was performed on a PC with a CPU Intel Core i7 (1.8 GHz, four cores) with 12 GB RAM. After three weeks of numerical calculation, it converged at the 43rd generation with 100 parameter design candidates in each generation, as shown in Figure 7. During CFD analysis, the average velocity oscillates along the converging line, which maintains consistent, optimized parameters, showing a maximum velocity output difference of 0.000916 m/s. The computational domain treats the thruster, setting the static fluid domain to mimic the conditions of a large water area. The analysis also examines varying flow speed outputs using CFD techniques.

The three-week optimization period reflects the cumulative cost of 4,300 autonomous CFD evaluations (43 generations × 100 design candidates). While the absolute velocity improvement of 0.36 m/s represents a 7.13% gain, the fully automated GA-CFD framework requires no human intervention once initiated, making the computational investment practical for systematic design exploration.

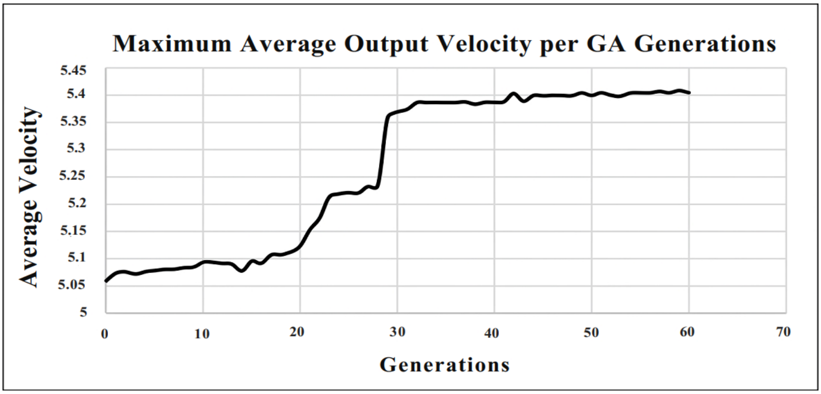

Figure 7. GA convergence curve

The GA's generation of new design candidates determines the analysis of the thruster's output speed. Consequently, Figure 8 displays the optimized parameters for the thruster's nose cone shape. The location for measuring output velocity is at the propeller disk's backplane, ensuring accurate measurement of the water's average output flow speed with each introduction of a new cone shape candidate. Table 3 shows the top three design parameters before and during the GA's stopping criterion.

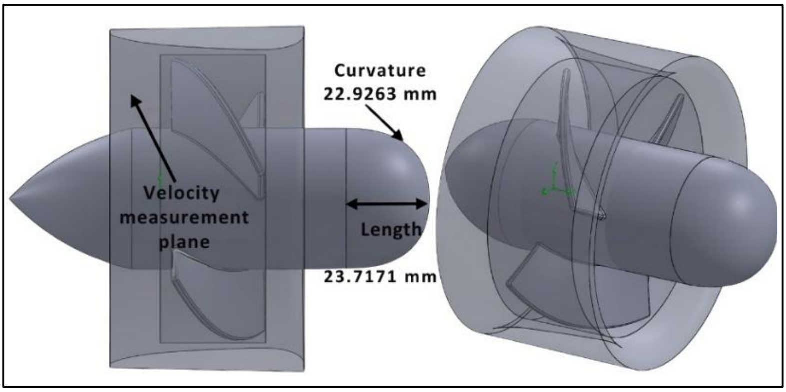

Figure 8. Optimized nose cone shape

The new nose cone shape proposed for the underwater thruster differs from the pointed design shown in the previous study (Huynh, 2016) for a thruster solution design. However, it is necessary to consider other candidates that can achieve a similar average outflow velocity. Table 3 shows three different nose cone shape candidates, with Design Candidate 3 identified as the configuration with the highest output velocity among the evaluated candidates. This configuration features a 22.9263 mm nose curve and a 23.7171 mm nose cone length. With an output velocity of 5.40522 m/s, this configuration achieved the highest output velocity among the evaluated candidates.

Table 3. Comparison of the intermediate and best-performing nose cone configurations

Design classification	Candidate	Nose Cone Profile	Generation Number	Curvature (mm)	Nose Cone Length (mm)	Output Velocity (m/s)
Intermediate design	1	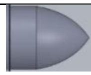	36	12.4237	23.7171	5.38102
Intermediate design	2	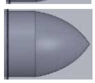	41	12.5397	23.7171	5.38361
Best-performing design	3	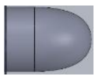	43	22.9263	23.7171	5.40522

The final best-performing configuration was identified in the 43rd generation. Shape 1 represents the first-best intermediate design candidate for the nose cone curve, with a value of 12.4237 mm, yielding an output speed of approximately 5.38102 m/s. Nose cone shape number 2 emerges as the second-best intermediate design candidate, with a nose curve of 12.5397 mm and an output velocity of 5.38361 m/s. Both intermediate best designs share the same nose cone length of 23.7171 mm.

Figure 9 in the study shows how water flows through the AUV's nose cone system, moving from the entry point through the propeller and exiting the thruster. This visualization, obtained from computational fluid dynamics analysis, clearly shows how the fluid moves during this process. By optimizing the shape of the nose cone, the flow improves, resulting in an output velocity of around 5.4 meters per second at the plane measurement, as outlined in Table 3. This higher velocity suggests a more efficient propulsion system for the AUV.

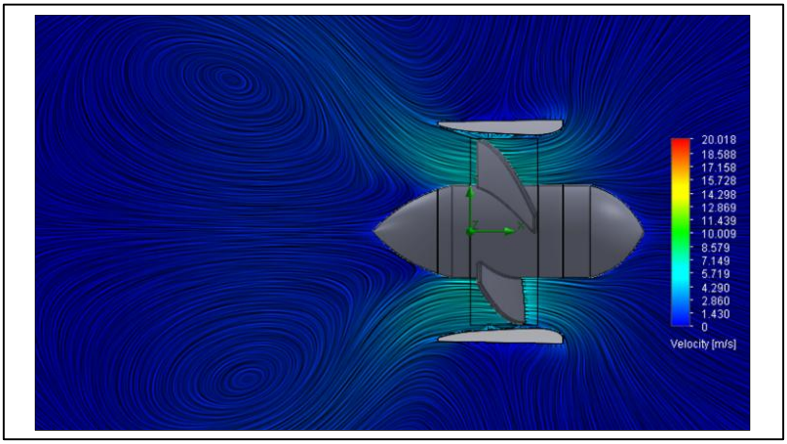

Figure 9. Streamlines of velocity around the thruster

3.1 Grid-sensitivity Results

Table 4 presents the results of the grid-sensitivity assessment conducted using Design Candidate 3.

Table 4. Grid-sensitivity assessment of Design Candidate 3

Mesh level	Global mesh divisions	Fluid cells	Solid-contact cells	Average output velocity (m/s)	Difference from finer mesh (%)
Coarse	24 × 24 × 24	17,308	884	5.28318	3.03
Medium	32 × 32 × 32	39,523	1,481	5.44810	5.74
Fine	43 × 43 × 43	88,540	2,802	5.15233	—

Increasing the grid density from the coarse to the medium mesh changed the predicted average output velocity by 3.03%, while refinement from the medium to the fine mesh resulted in a 5.74% difference. All three simulations satisfied the prescribed surface-goal convergence criterion. However, the predicted velocities did not vary monotonically with successive grid refinement. The results therefore indicate that the predicted output velocity remains sensitive to mesh resolution and that strict asymptotic mesh independence was not fully established within the three investigated mesh levels.

The original GA–CFD optimization employed the SOLIDWORKS automatic meshing procedure consistently for all generated design candidates. Under this common numerical framework, Design Candidate 3 achieved an average output velocity of 5.41 m/s and was identified as the best-performing nose cone geometry in terms of output velocity within the investigated design space. The subsequent manual-mesh simulations were performed as a post-optimization grid-sensitivity assessment and did not constitute a new optimization process. Accordingly, the original automatic-mesh value is retained as the reported GA optimization result. Further verification using localized refinement around the propeller blades, nose cone surface, rotating-region interface, and velocity-measurement plane is recommended to establish asymptotic grid convergence.

4. Conclusions and Recommendation

This study demonstrated that an automated genetic algorithm–computational fluid dynamics (GA-CFD) framework can effectively optimize thruster nose-cone geometry to enhance hydrodynamic performance. The optimization identified the best-performing configuration within the investigated design space, with c = 22.93 mm and l = 23.72 mm, which increased the thruster output velocity from approximately 5.05 m/s to 5.41 m/s, corresponding to a 7.13% improvement. The optimized geometry exhibited a more rounded profile than the pointed configuration of the original T200 thruster nozzle reported by Huynh (2016), indicating that conventional pointed designs may not be the most favorable for maximizing output flow velocity. In addition, the fully automated MATLAB-SOLIDWORKS-GA-CFD workflow achieved convergence at the 43rd generation after 4,300 CFD evaluations, confirming the feasibility of autonomous optimization for thruster component design. Overall, the findings show that coupling GA with CFD in an integrated automated framework provides a practical and effective approach for the data-driven refinement of underwater propulsion components. The optimization was limited to average output velocity as a single-objective fitness measure. Consequently, the identified geometry should not be interpreted as maximizing the overall performance of the thruster, since thrust, propulsive efficiency, pressure loss, torque, power consumption, and cavitation were not directly evaluated. Future studies should adopt a multi-objective optimization framework that considers these parameters together with output velocity to establish a more comprehensive thruster design. Future work should focus on experimental validation of the optimized design, extension of the optimization to additional geometric parameters such as the tail section and duct profile, and evaluation under varying inlet velocity and depth-dependent operating conditions.

Nomenclature:

T – Thrust (N); Q – Volume flow rate (m^3/s);
VP – velocity through the propeller disk (m/s);
AP – Propeller disk area (m^2);
UA – Added velocity (m/s);
l – Nose cone length (mm);
c – Spline curvature (mm);
ρ – Fluid density (kg/m^3);
μ – Dynamic viscosity (Pa·s);
Re – Reynolds number;
GA – Genetic Algorithm;
CFD – Computational Fluid Dynamics;
AUV – Autonomous Underwater Vehicle;
USV – Unmanned Surface Vehicle;
MRF – Moving Reference Frame;
RPM – Revolutions per minute

5. References

Bhuiyan, S.A., Hasan, M.J., & Hoque, M.A. (2025). Enhancing hydrodynamic efficiency in Autonomous Underwater Vehicles (AUVs) utilizing adjoint method and proper orthogonal decomposition. *PLoS ONE, 20*(3). https://doi.org/10.1371/journal.pone.0319321

Blue Robotics. (2017). T200 Thruster. https://bluerobotics.com/store/thrusters/t100-t200-thrusters/t200-thruster-r2-rp/

Chung, H.K., & Kim, J. (2013). Analysis of underwater thruster model with ambient flow velocity using CFD. *Intelligent Service Robotics, 6*(3), 163–168. https://doi.org/10.1007/s11370-013-0133-7

Dassault Systèmes. (2021). SOLIDWORKS with SOLIDWORKS Flow Simulation [Computer software]. Vélizy-Villacoublay, France: Dassault Systèmes.

Dassault Systèmes. (2021). SOLIDWORKS flow simulation technical reference. Retrieved from https://www.cati.com/wp-content/uploads/2021/04/swflow2021-technical-reference.pdf

Divsalar, K. (2020). Improving the hydrodynamic performance of the SUBOFF bare hull model: A CFD approach. *Acta Mechanica Sinica/Lixue Xuebao, 36*(1), 44–56. https://doi.org/10.1007/s10409-019-00913-7

Han, J., Park, J., Kim, J., & Son, N. S. (2016). GPS-less coastal navigation using marine radar for USV operation. *IFAC-PapersOnLine, 49*(23), 598–603. https://doi.org/10.1016/j.ifacol.2016.10.500

Huynh, J.Q.T. (2016). *Detailed design of a thruster solution for a small mass-market remotely operated underwater vehicle (Master's thesis).* Norwegian University of Science and Technology, Trondheim, Norway. https://hdl.handle.net/11250/2416482

Joung, T.H., Choi, H.S., Jung, S.K., Sammut, K., & He, F. (2014). Verification of CFD analysis methods for predicting the drag force and thrust power of an underwater disk robot. *International Journal of Naval Architecture and Ocean Engineering, 6(2), 269–281*. https://doi.org/10.2478/IJNAOE-2013-0178

Kartha, J.J., & Jacob, L. (2015). Delay and lifetime performance of underwater wireless sensor networks with mobile element based data collection. *International Journal of Distributed Sensor Networks, 2015*. https://doi.org/10.1155/2015/128757

Kotragouda, N.B. (2007). Application of genetic algorithms and CFD for flow control. Master's Thesis. University of Kentucky, Lexington, Kentucky, USA. https://uknowledge.uky.edu/gradschool_theses/451

Lam, J., Chen, A., Bennett, A., & Triantafyllou, M. (2023). Propeller characterization testing of a blue robotics T200 thruster. In *OCEANS 2023–Limerick* (pp. 1–8). IEEE. https://doi.org/10.1109/OCEANSLimerick52467.2023.10244513

Lidtke, A.K., Turnock, S.R., & Downes, J. (2018). Hydrodynamic design of underwater gliders using k-kL-ω Reynolds averaged Navier-Stokes transition model. *IEEE Journal of Oceanic Engineering,* 43(2), 356–368. https://doi.org/10.1109/JOE.2017.2733778

Liu, T., Liu, Y., Zhang, L., Zhang, H., Wu, Z., & Wang, Y. (2017). Hydrodynamic shape genealogy for teardrop-shaped Autonomous Underwater Vehicles. OCEANS 2017 - Aberdeen, 2017, 1–6. https://doi.org/10.1109/OCEANSE.2017.8084736

Luo, H., Wu, K., Ruby, R., Hong, F., Guo, Z., & Ni, L. M. (2017). Simulation and experimentation platforms for underwater acoustic sensor networks: Advancements and challenges. *ACM Computing Surveys, 50*(2). https://doi.org/10.1145/3040990

Maruyama, K., & Yoshikawa, T. (2018). Acquiring multiple satisfied solutions in a unified objective optimization problem. Proceedings - 2018 joint 10th international conference on soft computing and intelligent systems and 19th international symposium on advanced intelligent systems, SCIS-ISIS 2018, 103–108. https://doi.org/10.1109/SCIS-ISIS.2018.00028

Masmitja, I., Gonzalez, J., Galarza, C., Gomariz, S., Aguzzi, J., & del Rio, J. (2018). New vectorial propulsion system and trajectory control designs for improved AUV mission autonomy. *Sensors (Switzerland), 18*(4), 1–26. https://doi.org/10.3390/s18041241

Matias, B., Oliveira, H., Almeida, J., Dias, A., Ferreira, H., Martins, A., & Silva, E. (2015). High-accuracy low-cost RTK-GPS for an unmannned surface vehicle. MTS/IEEE OCEANS 2015 - Genova: Discovering Sustainable Ocean Energy for a New World, (May). https://doi.org/10.1109/OCEANS-Genova.2015.7271673

Saghafi, M., & Lavimi, R. (2020). Optimal design of nose and tail of an autonomous underwater vehicle hull to reduce drag force using numerical simulation. Proceedings of the Institution of Mechanical Engineers Part M: *Journal of Engineering for the Maritime Environment, 234*(1), 76–88. https://doi.org/10.1177/1475090219863191

The MathWorks, Inc. (2018). MATLAB (Version R2018b) with Global Optimization Toolbox [Computer software]. Natick, Massachusetts, United States: The MathWorks, Inc.

Vasudev, K.L., Sharma, R., & Bhattacharyya, S.K. (2018). Shape optimisation of an AUV with ducted propeller using GA integrated with CFD. *Ships and Offshore Structures*, *13*(2), 194–207. https://doi.org/10.1080/17445302.2017.1351292